Available online at www.sciencedirect.com
ScienceDirect
Infrared Physics & Technology 50 (2007) 142–148
INFRARED PHYSICS & TECHNOLOGY
www.elsevier.com/locate/infrared

Performance improvements of ultraviolet/infrared dual-band detectors

A.G.U. Perera [a,*], G. Ariyawansa [a], M.B.M. Rinzan [a], M. Stevens [a], M. Alevli [a], N. Dietz [a], S.G. Matsik [b], A. Asghar [c], I.T. Ferguson [c], H. Luo [d], A. Bezinger [d], H.C. Liu [d]

[a] *Department of Physics and Astronomy, Georgia State University, Atlanta, GA 30303, United States*
[b] *NDP Optronics, Mableton, GA 30126, United States*
[c] *School of Electrical and Engineering, Georgia Institute of Technology, Atlanta, GA 30332, United States*
[d] *Institute for Microstructural Sciences, National Research Council, Ottawa, Canada K1A OR6*

Available online 13 November 2006

Abstract

Results are reported on dual-band detectors based on a GaN/AlGaN structure operating in both the ultraviolet–midinfrared (UV–MIR) and ultraviolet–farinfrared (UV–FIR) regions. The UV detection is due to an interband process, while the MIR/FIR detection is from free carrier absorption in the emitter/contact followed by internal photoemission over the barrier at the GaN/AlGaN interface. The UV detection, which was observed from 300 K to 4.2 K, has a threshold of 360 nm with a peak responsivity of 0.6 mA/W at 300 K. The detector shows a free carrier IR response in the 3–7 μm range up to 120 K, and an impurity response around 54 μm up to 30 K. A response in the range 7–13 μm, which is tentatively assigned to transitions from C impurities and N vacancies in the barrier region, was also observed. It should also be possible to develop a detector operating in the UV–visible–IR regions by choosing the appropriate material system. A dual-band detector design, which allows not only to measure the two components of the photocurrent generated by UV and IR radiation simultaneously but also to optimize the UV and IR responses independently, is proposed.

PACS: 73.30.+y; 85.60.Bt; 85.60.Gz; 73.61.Ey; 78.20.Ci; 81.05.Ea; 71.55.Eq

Keywords: Dual-band detector; GaN/AlGaN; IR detectors; UV detectors

1. Introduction

Several dual-band detectors [1–3] based on group III-As material systems, operating in near-infrared (NIR), and mid-/very-long-wavelength-/far-infrared (MIR/VLWIR/FIR) regions have been reported. Recently, homojunction device structures based on GaAs [4] and Si [5] having a dual-band response in NIR and VLWIR have also been demonstrated. GaN dual-band detectors [6] reported so far can detect ultraviolet (UV) and NIR radiation. Detecting multiple wave bands by a single detector can eliminate the difficulties of operating several detectors with separate cooling assemblies and electronics. One example of UV/IR dual-band detector is fire and flame detection where different types of fires emit different radiation strengths from UV to IR. Different flames from different materials, such as hydrogen and coal, have significant intensity variation in the emission spectrum in the UV and IR regions. Moreover, these detectors can be used as UV or NIR detectors alone, and can be employed in applications in the same way as other IR detectors. Group III-Nitrides, especially GaN, have become the material of interest in developing high speed electronic and optoelectronic devices, other than the well studied group III-Arsenides such as GaAs. Ultraviolet (UV) detectors [7,8], UV light emitting diodes [9–11] and laser diodes [12] have been successfully demonstrated, and are widely available for commercial applications such

* Corresponding author. Tel.: +1 404 651 2847; fax: +1 404 651 1427.
E-mail address: uperera@gsu.edu (A.G.U. Perera).

1350-4495/$ - see front matter © 2006 Elsevier B.V. All rights reserved.
doi:10.1016/j.infrared.2006.10.013

as flame detection, UV imaging, solar UV detection, as well as applications for industries such as those focusing on military, agricultural, and automotive products. In the range of infrared, researchers have reported GaN/AlGaN Schottky photodiodes [13] and quantum well infrared photodetectors (QWIPs) [14]. In the FIR region, one advantage of GaN over GaAs is that GaN has higher absorption than GaAs, and also the reststrahlen region of GaAs can be accessed with GaN, gaining a broad response from 20 μm and above. Another advantage is detecting both UV and IR radiation simultaneously, which would be an important tool in fire fighting, and for military and other applications. Moreover, the wide band gap of GaN reduces interband tunneling relative to GaAs, and the higher effective mass would reduce the thermal emission. However, development of GaN high speed optoelectronic devices with improved performance are still in their infancy since the growth of high-quality GaN/AlGaN heterostructures is limited by the availability of suitable lattice-matched substrate materials and process/material knowledge base. Here, the successful results on a HEterojunction Interfacial Workfunction Internal Photoemission (HEIWIP) detector based on GaN/AlGaN system, which can be operated in both UV and IR (3–13, and 20–70 μm) regions, is reported. A design for a UV/IR dual-band detector with improved detector performance and simultaneous dual-band detection capability is proposed.

2. Experiment

The HEIWIP structure was grown by organometallic chemical vapor deposition (OMCVD) on sapphire substrate, and consists of a Si doped n^+ GaN emitter layer (also served as the top-contact), an undoped $Al_{0.1}Ga_{0.9}N$ barrier, and a n^+ GaN bottom contact layer, as shown in Fig. 1(a). The thickness and the doping density of the GaN emitter, and the GaN bottom-contact are 0.2 μm, 5×10^{18} cm^{-3}, 0.7 μm, 5×10^{18} cm^{-3}, respectively, and the thickness of the undoped $Al_{0.1}Ga_{0.9}N$ barrier is 0.6 μm. The structure was processed to form square mesa elements with different active areas by dry etching techniques. The ohmic contacts were formed by deposition of Ti/Al/Ti/Au (metalization) on the top- and bottom-contact layers. After the metalization, the device structure was annealed under a N_2 gas flow at 700 °C temperature for two minutes. The annealed sample was mounted on chip carriers and wire bonds were made from each mesa of the sample to the chip carrier. Current–voltage (*IV*) measurements were performed, by using a Keithley 2400 source meter, on all the mesas of the sample in order to check for uniformity of the structure. The spectral response of the detector in the UV region was obtained using an Oriel Deuterium UV source, UV/VIS monochromator, and neutral density filters, and spectra were calibrated using a background spectrum obtained by a Hamamatsu photomultiplier tube with a known sensitivity. Spectral measurement in the IR region for normal incidence radiation was carried out by using a Perkin Elmer System 2000 Fourier transform infrared (FTIR) spectrometer. The spectra were calibrated relative to a background spectrum obtained by a Si composite bolometer with the same set of optical components.

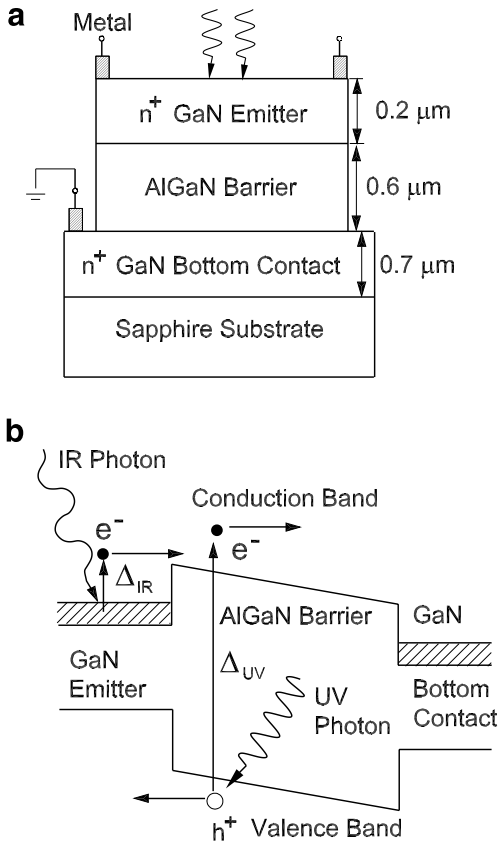

Fig. 1. (a) Schematic diagram of GaN/AlGaN HEIWIP structure. The doping concentration of the GaN emitter and the bottom-contact is 5×10^{18} cm^{-3}. The $Al_{0.1}Ga_{0.9}N$ barrier is not intentionally doped. (b) Band diagram showing the conduction band profile. The interband transition in the barrier leads to UV response, while IR response is due to intraband transition. The band offset Δ determines the wavelength threshold.

3. Results and discussion

The dual-band detection involves two detection mechanisms. The energy band diagram indicating the transitions due to both mechanisms is depicted in Fig. 1(b). The UV detection is based on interband transitions of carriers in the $Al_{0.1}Ga_{0.9}N$ barrier. The intraband detection (IR) mechanism involves free carrier absorption in the emitter, followed by the internal photoemission of photoexcited carriers across the junction barrier, and then the collection of carriers by the applied electric field at the contacts. The offset between the Fermi level in the emitter layer and the valence band edge of the barrier layer forms the interfacial workfunction (Δ) which arises due to the band offset of different materials [15], and the band gap narrowing [16] of the highly doped emitter layer. The threshold wavelength λ_0 (μm) is given by $1240/\Delta$, where Δ is in meV. A comparison of the calculated IR absorption of 1 μm thick

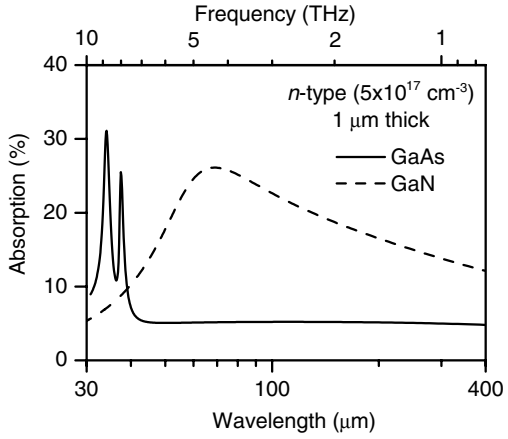

Fig. 2. A comparison of the calculated IR absorption of 1 μm thick 5×10^{17} cm^{-3} n-doped GaAs and GaN films in the IR region.

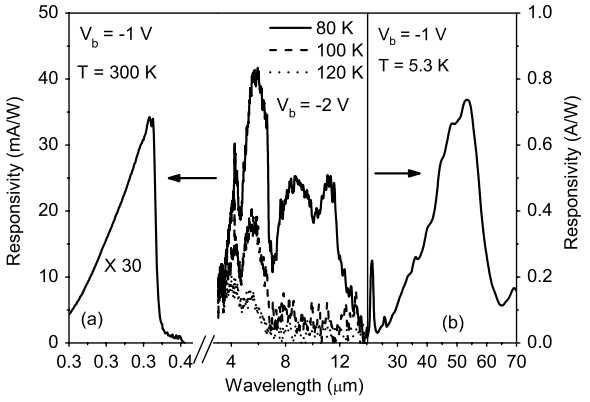

Fig. 4. (a) UV/IR dual-band response of the detector. The UV responsivity curve has been multiplied by 30 for clarity. (b) The response at 54 μm (5.5 THz), which is due to the transition between 1s and 2p± impurity levels of Si in GaN.

5×10^{17} cm^{-3} n-doped GaAs and GaN films is shown in Fig. 2. As seen in the figure, due to higher absorption in the region above 40 μm, GaN would be a good candidate for the FIR detector development.

The dark current of the detector at different temperatures is shown in Fig. 3. The detector shows a higher dark current than other detectors operating in similar regions. This increase in the dark current is possibly ascribed to the hopping conductivity of Si impurity electrons in the barrier. The presence of Si impurities has been confirmed by a response peak at ~54 μm corresponding to photoionization of Si impurity atoms, which will be discussed later.

The UV/IR dual-band response of the detector is shown in Fig. 4(a). UV photons excite the valance electrons in the AlGaN barrier layer, and the generated electron-hole pairs are separated by the applied electric field before recombination, as shown in Fig. 1(b). The UV threshold wavelength observed at 360 nm matches the band gap of $Al_{0.1}Ga_{0.9}N$ alloy. Due to autodoping in GaN, it is expected that the barrier region will be n-doped to ~10^{17} cm^{-3} even though no intentional doping was carried out. This autodoping may enhance the UV detection by increasing the gain in the UV detector due to trapping of minority carriers at the interface [17]. The bandgap between the valence and conduction bands in $Al_{0.1}Ga_{0.9}N$ is $E_G = 6.13x + 3.42(1-x) - 1.08x(1-x)$ eV [18], where x is the Al fraction in the AlGaN barrier. The UV threshold wavelength λ_{0G} (nm) is then given by $\lambda_{0G} = 1240/E_G$ where E_G is in eV. The free carrier absorption occurs in the emitter layer and carriers undergo photoemission across the barrier (Fig. 1(b)). The detector shows a free carrier response in the 3–7 μm range, and the response can be observed up to 120 K.

The experimental responsivity of the detector in both UV and IR regions are fitted to theoretically expected responses, as shown in Fig. 5. The permittivity associated with the interband transition is calculated by using the model dielectric function [19]. The permittivity for the intraband transition is calculated by using a model [15] based on Lorentz–Drude theory. The light propagation in the structure is derived from the transfer matrix method. The responsivity, R is given by $R = \eta g_p q\lambda/hc$, where η is the total quantum efficiency, g_p is the photoconductive gain, q is the electron charge, λ is the wavelength, h is the Planck constant, and c is the speed of light. In comparison with

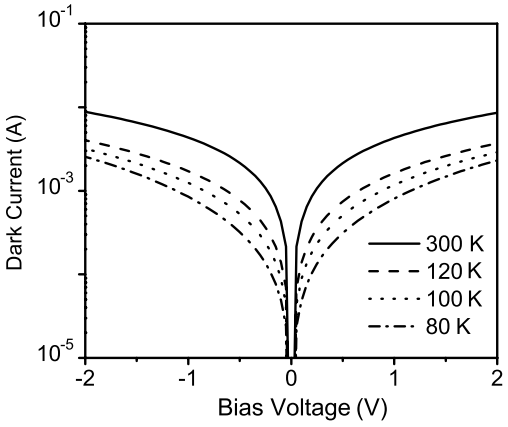

Fig. 3. Dark current of the GaN/ALGaN HEIWIP detector at different temperatures.

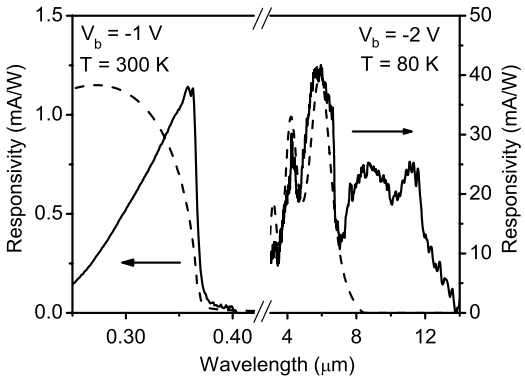

Fig. 5. Calculated UV/IR responses (dash line) of the detector, fitted with the experimental results (solid line).

the model response, the UV responsivity decreases with decreasing wavelength below the band edge. This effect and possible causes have been reported previously [20]. The IR response consists of a free carrier response, which matches the calculated response, and an impurity-related response. The oscillations in the response spectrum can be fitted with Fabri–Perot interference in the structure. The experimental and calculated thresholds of the detector reported in this article and a similar $GaN/Al_{0.026}Ga_{0.974}N$ detector reported previously [21] in both UV and IR regions is shown in Fig. 6.

The detector shows a distinguishable IR response in the two regions, 3–7 μm and 7–13 μm. The short region response 3–7 μm is the expected free carrier response as designed, while the response in the region 7–13 μm could be due to impurity-related transitions in the structure, potentially due to C impurities or the N vacancies. The reported donor ionization energy of carbon [22] falls in the 110–140 meV range, while the binding energy of N vacancy [23] is about 100 meV. Hence, the two peaks observed at 9 and 11 μm (138 and 113 meV, respectively) could be due to transitions between carbon impurity states. Furthermore, the free carrier response was observed up to 120 K, as shown in Fig. 4(a), and the response in the range 7–13 μm drastically decreased with increasing temperature. This temperature dependent variation is good evidence that the responses in the two regions are connected to two different mechanisms. The lower temperature for the impurity is associated with the lower energy required for thermal excitation, depleting the impurity states.

A sharp peak at 54 μm (5.5 THz), which corresponds to an energy of 23 meV for the transition leading to it, is observed in the response spectrum, as shown in Fig 4(b). Wang et al. [24] reported the donor binding energy of Si in GaN to be 29 meV, and the transition from 1s to 2p± level occurs at 21.9 meV. Moore et al. [25] reported the 1s–2p± transition of Si in GaN at 23.3 meV, and donor effective mass binding energy of 31.1 meV. Hence, it can be concluded that the sharp response peak observed at 23 meV is due to 1s–2p± transition of Si donors in GaN. This concludes that GaN offers the possibility of developing a 5.5 THz (54 μm) detector, based on the 1s–2p± transition of Si in GaN. On the other hand, the Si impurity-related transition can lead to an increased dark current for a detector designed to operate in a shorter wavelength region. A similar response was also reported for the previous $GaN/Al_{0.026}Ga_{0.974}N$ HEIWIP detector [21].

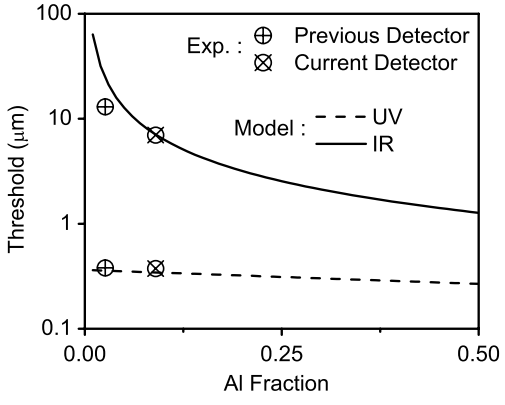

Fig. 6. Experimental and calculated wavelength thresholds in UV and IR regions for the detector reported in this article (current) and the detector demonstrated previously [21].

In comparison with UV detectors, the reported GaN/AlGaN HEIWIP UV/IR dual-band detectors (previous [21] and current) have much lower UV responses. The probable cause for the low UV response is the high absorption of UV radiation within the 0.2 μm thick top-contact layer. The absorption coefficient for GaN is $>10^5\ cm^{-1}$, which means that in the 0.2 μm thick top-contact, the absorption would be 90% or greater. Also the carriers generated by the absorption of UV radiation in the top-contact do not contribute to the photocurrent. In order to eliminate the effect of the top-contact, another detector was fabricated from the same structure (the reported detector structure in this article) by etching the top-contact out, except directly under the metal ring, as shown in Fig. 7. However, this will lead to a reduced infrared detection under reverse bias (top-contact is negative) since there is no emitter region for free carrier absorption. In the later part of the discussion, the labels ''Unetched'' and ''Etched'' will be used to refer to the original detector and the detector after etching the top-contact, respectively. In the etched-structure, UV radiation is directly incident onto the barrier layer, and a maximum absorption of UV radiation can be expected.

As shown in Fig. 8, the dark current of the etched-detector has decreased by an order of magnitude. Since the

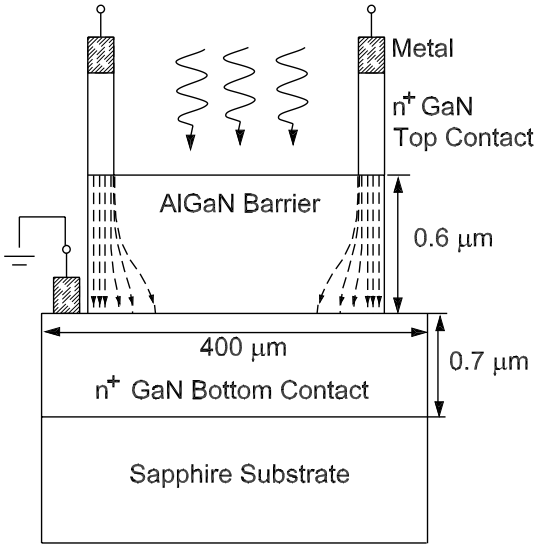

Fig. 7. Schematic diagram of GaN/AlGaN HEIWIP structure after etching the top-contact except under the metal ring. UV radiation is directly incident onto the barrier and absorption takes place mainly in the barrier. The electric field distribution in the barrier under positive bias (top-contact is positive) is also shown.

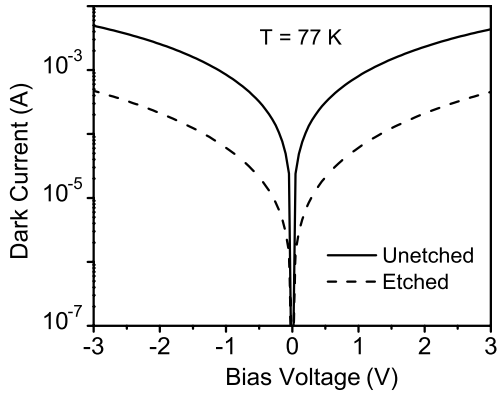

Fig. 8. Comparison of the dark current of the unetched- and etched-detectors. Since the top-contact has been removed inside the metal ring, the effective electrical area of the device has reduced, leading to a higher resistance, and hence lower dark current.

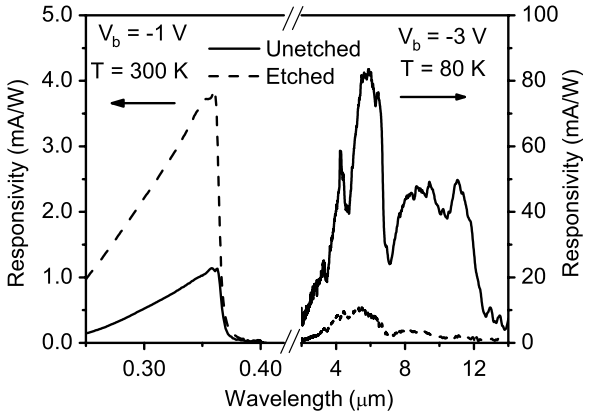

Fig. 9. Comparison of UV/IR dual-band response of both unetched- and etched-detectors. By etching the top-contact, the UV response was enhanced by a factor of 4, while the IR response was reduced by a factor of 8.

top-contact has been removed inside the metal ring, the effective electrical area of the device has reduced, leading to a higher resistance, and hence lower dark current. A comparison of the UV–IR dual-band response of both unetched and etched-detector is shown in Fig. 9. The UV response is at 300 K under −1 V bias, while the IR response is at 80 K under −3 V bias, and both samples were measured in a single run to minimize any change in the measurement setup. By etching the top-contact, the UV response was enhanced by a factor of 4, while the IR response was reduced by a factor of 8. For the etched-detector, even though the absorption in the barrier layer is high, the expected enhancement was not achieved. It could be due to reduced collection efficiency of the excited carriers as a result of non-uniform electric field distribution in the barrier and hence the weak field in the middle of the barrier, as shown in Fig. 7. The IR response of the unetched-detector has reduced significantly, however, there is still non-zero IR response due to impurity transitions in the barrier and the portion of the top-contact left in the structure.

While the dual-band detector reported here are detecting both UV and IR radiation, the two components of the photocurrent generated by UV and IR radiation cannot be separated out unless external optical filters are used. Using external optical filtering can reduce the radiation intensity incident onto the detector, and hence decrease the performance of the device. As the response for the two processes originate at different locations, it will be possible to design a device that is capable of separately measuring both components of the photocurrent simultaneously. The idea is to use three contacts to measure two separate currents simultaneously, and then from these currents to separate the UV and IR contributions. The processed device structure and the conduction/valence band profile for the proposed design are shown in Figs. 10, and 11, respectively. The expected wavelength thresholds in the UV and IR regions are 350 nm and 14 μm, respectively. The photocurrent generated by IR radiation can be measured with the middle- and bottom-contacts (IR active region) under both forward and reverse bias. The UV skin-depth is smaller than the combined thickness of the UV active region and hence the intensity of UV radiation incident on to the IR active region is insignificant. As a result, UV absorption does not take place in the IR active region. The component of the photocurrent generated by UV radiation can be measured with top- and middle-contacts. Since the top-contact is etched out leaving just a ring-contact, there is no effective emitter–barrier junction when the top-contact is negatively biased. Therefore, under this configuration, there is no free carrier generated IR photocurrent expected in the UV active region.

The dual-band detection approach, reported in this article, can be used to develop dual-band detectors tailored to specific applications. By adjusting the material composition in the layers, the thresholds for the interband and intra-

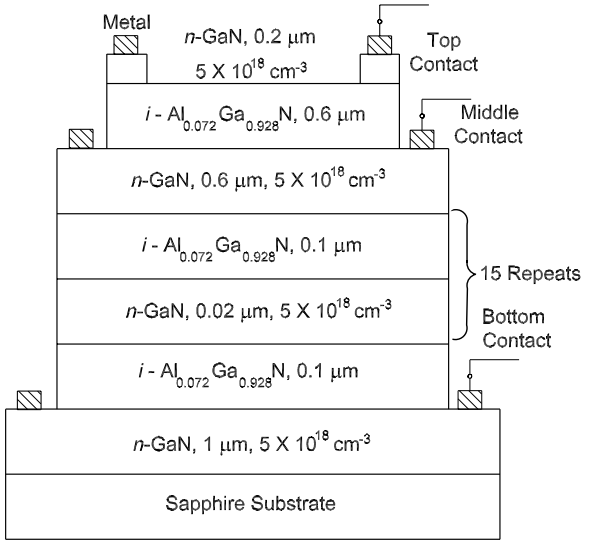

Fig. 10. Schematic diagram of a processed GaN/AlGaN HEIWIP detector structure designed for simultaneous measurement of the two components of the photocurrent generated by UV and IR radiation.

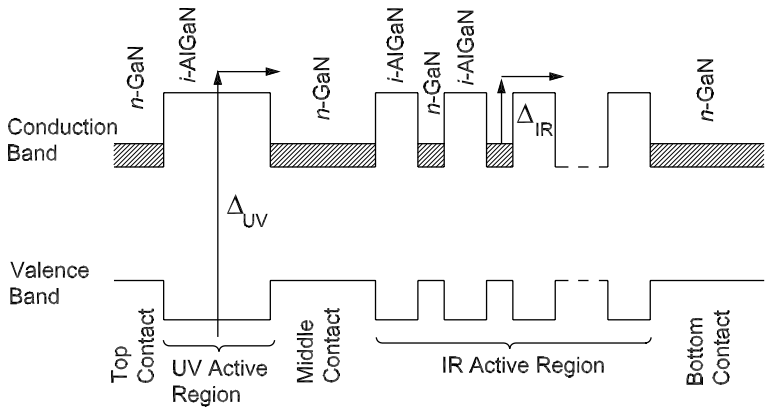

Fig. 11. Conduction and valence band profile of the proposed device structure designed for simultaneous measurement of the two components of the photocurrent generated by UV and IR radiation.

Table 1
Summary of different materials used to obtain dual-band response in different spectral regions

Barrier material	Emitter material	Interband response threshold (μm)	Free carrier response range (μm)
i-GaAs	p-GaAs	0.8	5–72
i-Si	p-Si	1.1	5–35
i-$Al_{0.1}Ga_{0.9}N$	n-GaN	0.360	3–7

GaAs [4] and Si [5] homojunction detectors have been reported previously.

band responses can be tailored separately. For example, in an AlGaN based detector, if the Al fraction is varied in both the emitter and barrier by the same amount, only the interband threshold will change, while the intraband threshold remain constant. Alternatively varying only the emitter Al fraction, the intraband threshold could be varied without changing the interband threshold. Moreover, the resonant cavity effects can be used to tailor the IR response peak to the desired wavelength. By adjusting the materials it will be possible to tune the interband threshold from the UV to NIR and the intraband threshold from the MIR to the FIR. That is, the reported dual-band approach with HIWIP/HEIWIP detectors can be tested with any material such as InN, InGaN, GaN, AlGaN, and AlN. InN could give an interband response in NIR, while InGaN could respond in NIR–Visible (VIS) regions. A UV interband response could be expected from an AlN based detector. A summary of different materials used to develop dual-band detectors is shown in Table 1, which includes both homojunction and heterojunction detectors.

4. Summary

In summary, GaN/AlGaN HEIWIP dual-band detectors responding in UV and IR regions based on interband and intraband transitions in the structure are reported. The UV threshold is observed at 360 nm, and the IR response is in the range 3–13 μm. A response at 54 μm is also observed, which is due to the transition between 1s and 2p± impurity levels of Si in GaN. Based on theoretical models and experimental data, the transitions leading to each band are explained. The weak UV response of the detector is due to the high absorption of UV radiation in the top-contact layer, which does not contribute to photocurrent. By etching out the top-contact layer, it is shown that the UV response of the detector can be enhanced. A dual-band detector design, which can be used to measure the two components of the photocurrent generated by UV and IR radiation simultaneously, is also proposed. Moreover, this design allows to optimize the UV and IR responses independently. By adjusting the material or the alloy fraction, the threshold wavelength of the interband, and intraband responses can be tailored.

Acknowledgements

This work is supported in part by the US Air Force Small Business Innovation Research Program (SBIR) under grant no: FA9453-05-M-0106. The authors would like to acknowledge Dr. Dave Cardimona and Dr. Tzveta Apostolova for fruitful discussions and the support, and Rongzhu Wang and Hun Kang for technical assistance.

References

[1] Arnold Goldberg, Parvez N. Uppal, Michael Winn, Infrared Phys. Technol. 44 (2003) 427.
[2] H.C. Liu, C.Y. Song, A. Shen, M. Gao, Z.R. Wasilewski, M. Buchanan, Appl. Phys. Lett. 77 (2000) 2437.
[3] M.P. Touse, G. Karunasiri, K.R. Lantz, H. Li, T. Mei, Appl. Phys. Lett. 86 (2005) 093501.
[4] G. Ariyawansa, M.B.M. Rinzan, D.G. Esaev, S.G. Matsik, A.G.U. Perera, H.C. Liu, B.N. Zvonkov, V.I. Gavrilenko, Appl. Phys. Lett. 86 (2005) 143510-3.
[5] G. Ariyawansa, M.B.M. Rinzan, S.G. Matsik, G. Hastings, A.G.U. Perera, H.C. Liu, M. Buchanan, G.I. Sproule, V.I. Gavrilenko, V.P. Kuznetsov, Appl. Phys. Lett. 89 (2006) 061112.
[6] D. Starikov, C. Boney, R. Pillai, A. Bensaoula, Sensors for Industry Conference 2004, in: Proceedings the ISA/IEEE, New Orleans, LA, USA, 2004, pp. 36–40.
[7] M. Asif Khan, J.N. Kuznia, D.T. Olson, M. Blasingame, A.R. Bhattarai, Appl. Phys. Lett. 63 (1993) 2455.

[8] D. Walker, X. Zhang, P. Kung, A. Saxler, S. Javadpour, J. Xu, M. Razeghi, Appl. Phys. Lett. 68 (1996) 2100.
[9] Madalina Furis, A.N. Cartwright, Hong Wu, William J. Schaff, Appl. Phys. Lett. 83 (2003) 3486.
[10] S.K. Zhang, W.B. Wang, I. Shtau, F. Yun, L. He, H. Morko, X. Zhou, M. Tamargo, R.R. Alfano, Appl. Phys. Lett. 81 (2002) 4862.
[11] J.P. Zhang, X. Hu, Yu. Bilenko, J. Deng, A. Lunev, M.S. Shur, R. Gaska, M. Shatalov, J.W. Yang, M.A. Khan, Appl. Phys. Lett. 85 (2004) 5532.
[12] V.D. Jovanovic, D. Indjin, Z. Ikonic, P. Harrison, Appl. Phys. Lett. 84 (2004) 2995.
[13] N. Biyikli, T. Kartaloglu, O. Aytur, I. Kimukin, E. Ozbay, MRS Internet J. Nitride Semicond. Res. 8 (2003) 2.
[14] Claire Gmachl, Hock M. Ng, Alfred Y. Cho, Appl. Phys. Lett. 77 (2000) 334.
[15] D.G. Esaev, M.B.M. Rinzan, S.G. Matsik, A.G.U. Perera, J. Appl. Phys. 96 (2004) 4588.
[16] W.Z. Shen, A.G.U. Perera, H.C. Liu, M. Buchanan, W.J. Schaff, Appl. Phys. Lett. 71 (1997) 2677.
[17] O. Katz, V. Garber, B. Meyler, G. Bahir, J. Salzman, Appl. Phys. Lett. 80 (2002) 347.
[18] Ü. Özgür, G. Webb-Wood, H.O. Everitt, F. Yun, H. Morkoç, Appl. Phys. Lett. 79 (2001) 4103.
[19] Takahiro Kawashima, Hisashi Yoshikawa, Sadao Adachi, Shunro Fuke, Kohji Ohtsuka, J. Appl. Phys. 82 (1997) 3528.
[20] Dennis K. Wickenden, Zhenchun Huang, D. Brent Mott, Peter K. Shu, Johns Hopkins APL Techn. Digest 18 (1997) 217.
[21] G. Ariyawansa, M.B.M. Rinzan, M. Alevli, M. Strassburg, N. Dietz, A.G.U. Perera, S.G. Matsik, A. Asghar, I.T. Ferguson, H. Luo, A. Bezinger, H.C. Liu, Appl. Phys. Lett. 89 (2006) 091113.
[22] V. Bougrov, M. Levinshtein, S. Rumyantsev, A. Zubrilov, in: M.E. Levinshtein, S.L. Rumyantsev, M.S. Shur (Eds.), Gallium Nitride (GaN), John Wiley & Sons, Inc., NY, 2001, p. 1.
[23] M. Sumiya, K. Yoshimura, K. Ohtsuka, S. Fuke, Appl. Phys. Lett. 76 (2000) 2098.
[24] Y.J. Wang, R. Kaplan, H.K. Ng, K. Doverspike, D.K. Gaskill, T. Ikedo, I. Akasaki, H. Amono, J. Appl. Phys. 79 (1996) 8007.
[25] W.J. Moore, J.A. Freitas Jr., R.J. Molnar, Phys. Rev. B 56 (1997) 12073.